*"This is the pre-peer reviewed version of the following article: [B. Orazbayev, N. Mohammadi Estakhri, A. Alù, and M. Beruete, "Experimental Demonstration of Metasurface-Based Ultrathin Carpet Cloaks for Millimeter Waves," Adv. Opt. Mater., vol. 5, no. 1, p. 1600606, Jan. 2017.], which has been published in final form at [doi:10.1002/adom.201600606]. This article may be used for non-commercial purposes in accordance with Wiley Terms and Conditions for Self-Archiving."*

DOI: 10.1002/((please add manuscript number))
**Article type: Communication**

# Metasurface-based ultrathin carpet cloak for millimetre waves

*Bakhtiyar Orazbayev, Nasim Mohammadi Estakhri, Andrea Alù*[*]*, Miguel Beruete*[*]

B. Orazbayev, Dr. M. Beruete
Antennas Group-TERALAB
Universidad Pública de Navarra
Campus Arrosadía, 31006 Pamplona, Spain
E-mail: miguel.beruete@unavarra.es
Dr. M. Beruete
Institute of Smart Cities
Public University of Navarra
31006 Pamplona, Spain
N. Mohammadi Estakhri, Dr. A. Alù
Department of Electrical and Computer Engineering
The University of Texas at Austin
Austin, Texas 78712, USA

Keywords: invisibility cloaks; metasurfaces; full polarization

The possibility of making large objects undetectable has motivated significant research activities in the past decade. In its ideal operation, an electromagnetic cloak should be able to conceal an object within a wide operation bandwidth and a broad angular range, independently of the polarization of light. Although the first invisibility cloaks[1] did not fulfil these constraints, were bulky and targeted mostly the lower-frequency spectrum, these seminal research activities have inspired several follow-up experimental demonstrations, including visible light cloaks.[2,3] In this paper we report the design and experimental demonstration of a metasurface carpet cloak, which works in millimetre-wave range independently of polarization and with a relatively wide frequency and angular widths response. We demonstrate that this ultrathin $\lambda_0/19$ carpet cloak

based on a gradient metasurface design reduces the scattering from a $1.1\lambda_0$ object and opens interesting perspectives for the use of cloaks and metasurfaces in millimetre-wave and terahertz applications.

Most invisibility cloaks have been designed to date by either applying the transformation optics (TO)[4,5] or scattering cancellation techniques.[6,7] In TO cloaks, the concealed region is enclosed by an anisotropic cover that bends the light beam around it, making the object effectively invisible. These cloaks are usually quite thick, suffer from losses, and are challenging to build. In turn, the scattering cancellation technique provides simpler designs with a more robust performance, and, in case of the mantle cloak based on patterned metasurface, are extremely thin.[8,9] However, this technique is limited by the size of the cloaked objects[10] and in its simplest form can be only applied to objects with size comparable to the wavelength. For large objects the design becomes cumbersome due to the fact that the number of the scattering harmonics and therefore the number of cloaking layers increases with the size of the object, leading to similar complexities as the TO approach. The challenging requirements on the electromagnetic parameters imposed by TO can be relaxed when designing carpet cloaks[11] based on the quasi-conformal mapping technique.[11,12] In this case cloaking is achieved by tailoring the cloak material properties to effectively compress the volume of an object to an infinitesimally thick sheet over a ground plane. This transformation can be achieved with non-magnetic materials with an inhomogeneous permittivity. Low refractive index gradient materials have been explored to improve the impedance matching with free-space.[13]

Recently a metasurface, an artificially engineered ultrathin surface, has attracted a great interest since it provides a control over the electromagnetic wave by manipulating the local amplitude and phase of its field.[14–16] As result a different approach to cloaking has been explored, based on such gradient metasurfaces.[17–20] The cloaking performance is achieved by manipulating the phase of the reflected wave along the edge of the concealed volume. In this approach, the cloak is composed of an ultrathin gradient metasurface, artificially engineered with subwavelength

elements, that are tailored to control the phase of the reflected wave and restore the wavefront scattered from the object, emulating a flat ground plane. A metasurface cloak based on this principle has been experimentally demonstrated in optics,[21] showing good perspectives for such cloaking technique. Moreover, a recent experimental work on the metasurface based cloak in low band of microwave range demonstrated a possibility of the restoring not only the amplitudes and phases, but also the initial polarization.[22] Although for the higher frequencies the fabrication is more complicated, due to the smaller sizes of the metasurface elements, this method can also find appealing applications in other frequency ranges, such as the emergent millimetre-wave and THz bands. A polarization independent metasurface based cloaking device in these frequency ranges may be highly promising in a variety of sectors such as communication, security, military, space and biomedical applications.[23,24] Moreover, as mentioned above, a response independent of polarization is critical for real-life applications given that the polarization of the incident wave is usually unknown. In our previous work,[19] we numerically analysed a terahertz carpet cloak based on a gradient metasurface made of closed ring resonators. We demonstrated that such cloak is able to restore the wavefront and phase of the reflected beam, reducing the unwanted scattering from a bump. Here, we improved this theoretical design and experimentally realized a cloaking prototype operating at 80 GHz, demonstrating scattering cross-section reduction from a metallic bump over a ground plane, within a relatively wide range of angles and frequencies for both *TE* and *TM* incident polarizations.

**Figure 1** shows the metasurface cloak considered in this work. The object to be concealed is a triangular bump with height 4.1 mm ($1.1\lambda_0$) and long side 40 mm ($10.7\lambda_0$). The restoration of the scattered wavefront is achieved by compensating the phase difference $\delta$ between the waves reflected from the ground plane and the edge of the concealed object, calculated at each point of the bump's edge following the method originally envisioned in [18-21]:

$$\delta = \pi - 2k_0 h\cos\theta \quad (1)$$

where $k_0$ is the free space wave vector at the operation frequency, $h$ is the height of the point from the ground plane, and θ is the angle of incidence of the incident wave with respect to the ground plane normal. As shown in the bottom left inset of Figure 1a, the metasurface is composed of double coaxial metallic rings with total metal thickness 0.8 μm, period 400 μm ($\lambda_0/9$) and gap between rings 10 μm placed on a high resistivity silicon substrate ($\rho > 10000$ Ω·m) with thickness 200 μm ($\lambda_0/19$) (see Supporting Information for more details). This geometry was chosen to make the metasurface insensitive to the polarization of the incident wave.[18] The response of each unit cell was tuned by changing the radii of the rings. The amplitude and phase curves of the reflection coefficient as a function of the ring radius are shown in the bottom right inset of Figure 1a.

Due to availability and mechanical restrictions, the silicon thickness is different from the one used in ref. 19 (165 μm). Therefore, an additional optimization of the cloaking metasurface was performed for the new silicon thickness (200 μm), resulting in the new optimal cloaking metasurface configuration. The metasurface layers were fabricated by using a photolithography process followed by a lift-off technique to print the metallic rings on the silicon substrate (more fabrication details can be found in the Supporting Information). A photograph of the fully cloaked structure with the fabricated metasurface covering the triangular bump is presented in Figure 1b, along with a microscope picture showing details of the metallic rings.

To evaluate the cloaking performance, we used two different experimental setups (top right inset of Figure 1b): based on an ABmm vector network analyser (VNA) (setup 1) and an Agilent E3861C VNA (setup 2). In both setups the reflection coefficient at different angles was recorded in the range 75–95 GHz, using two corrugated high gain horn antennas as transmitter and receiver. The distance from the transmitting horn antenna to the sample was sufficient to ensure a uniform illumination of the sample, at the same time avoiding diffraction from the metallic plane edges (more details of the setups are given in the Supporting Information). In the

first study, *TE* polarization with incidence angle θ = 45° was used. In this configuration, we measured three samples: bare ground plane, metallic bump on the ground plane, and bump cloaked with the gradient metasurface.

The colour-maps of the reflected electric field distribution as a function of frequency and azimuth angle φ for all three cases are shown in **Figure 2**a-c. As expected, the electrically large bare bump strongly scatters the electric field, resulting in two additional high peaks on both sides of the main specular reflection for all measured frequencies. When the cloak is applied, these peaks are significantly suppressed (almost –20 dB for some angles, see Figure. 2d, h, where the experimental and numerical radiation patterns are shown for $f_c$ = 86 GHz and 80 GHz respectively), confirming the scattering reduction. These results are compared with numerical simulations done with CST Microwave Studio in Figure 2e-g (details about the numerical simulation setup are given in the Supporting Information). As observed, measurements and simulations are in good agreement. The experiment presents a slight blue-shift ($f_c \approx$ 86 GHz) with respect to the design (and also simulation) frequency ($f_c$ = 80 GHz). We attribute this shift to multiple factors, such as deviations in the gap between the rings and the thickness of the fabricated metallic rings, due to the tolerances in the fabrication process. From additional simulations, shown in the Supplementary **Figure S**1, it can be seen that the central frequency $f_c$ blue-shifts as the metal thickness is increased. Comparing the simulation results with those in Ref. 19 (that correspond to a substrate height of 165 μm) it is clear that the present cloak is still able to significantly reduce the scattering in almost the same frequency range, even though the substrate thickness and therefore the optimal cloaking metasurface are not the same. The most important difference is that the main beam shape is not ideally recovered (see Supplementary **Figure S**2).

Next, we analyse the cloaking performance under *TM*-polarization. The numerical and measured radiation patterns for all three cases are shown in **Figure 3**. In a similar way as for

*TE* incidence, the cloak is able to reduce the scattering from the metallic triangular bump in the same frequency range. Moreover, the agreement of measurements and simulation results (Figure 3e-g) is again excellent. The cloaking performance is slightly degraded in comparison with the *TE* case, see Figure 3d, h. In order to quantitatively assess this difference in performance we calculated the scattering gain for $\theta = 45^{\circ}$ and both polarizations, defined as the ratio between the total RCS of the cloaked and bare bump, using the procedure described in the Supporting Information. The results are shown in **Figure 4**a. In both cases a scattering reduction is clearly observed with a minimum scattering gain around 86 GHz for both *TE* and *TM* polarizations. In the *TE* case, it reaches –6.5 dB, whereas under *TM* incidence the minimum is less pronounced (around –4.5 dB), demonstrating slightly worse performance for this polarization. This degradation of performance can be due to the fact that in *TM*-polarization the design is more sensitive to the substrate thickness and the non-uniformity of the structure (which manifests itself at large incidence angles). Moreover, for a better performance in *TM* polarization one could use a more complicated structure, for instance, a pyramidal shape, which more accurately restores the phase distribution on the metasurface.[20,22] Additional simulations (not shown here) show that for the substrate thickness (165 μm) used in ref. 19 the cloaking performance for both polarizations is in better agreement for smaller incidence angles ($\theta < 45°$).

Finally, to evaluate quantitatively the bandwidth and angular span of the fabricated cloak, we measured the radar cross section (RCS) and from it we calculated the scattering gain $G(f, \theta)$ for an incidence angle ranging from 25º to 55º, focusing in this case on *TE* polarization. For this purpose, we used setup 2 and obtained the azimuthal distribution of the reflection coefficient for all three cases mentioned above. This information was converted to RCS using the radar range equation[25] (for details of the extraction procedure see Supporting Information). In Figure 4b the experimental scattering gain is shown as a function of frequency and incidence angle θ. In good agreement with the results obtained with setup 1 the RCS of the cloaked bump

is suppressed by over 6 dB around $f_c$ = 86 GHz and θ = 45°. As shown in Figure 4b, the cloak demonstrates a 5 dB RCS suppression within a relatively large fractional bandwidth (~8%) and angular span (~15°).

The presented results show that an ultrathin metasurface cloak ($\lambda_0/19$) operating at millimetre-wave frequencies can supress the scattering from a moderately large bump over a ground plane, independently of the incident polarization. The measured prototype demonstrates a relatively wide frequency range with fractional bandwidth of 8% and angular span of 15°. Although the triangular shape of the bump makes the cloak more sensitive to imperfections of the metasurface (especially on top of the structure), it greatly facilitates the fabrication process, making it more feasible for a practical implementation. This work also highlights the possibility of building polarization-independent practical cloaks for macroscopic objects that may work for unknown polarization and over a relatively wide angular and frequency ranges, and may be integrated in millimetre-wave applications, such as radar automotive systems or ultrahigh speed telecommunication systems. More broadly, since this metasurface cloak can be scaled up for THz band, our work shows how gradient metasurfaces may make a significant impact to control and tailor THz radiation and wave propagation, in a frequency range for which ultrathin components and devices are scarcely available and inefficient, and for which deeply subwavelength control may be routinely achieved with conventional fabrication processes.

**Supporting Information**
Supporting Information is available online from the Wiley Online Library or from the author.

**Acknowledgements**
Authors are grateful to Adrian Gomez Torrent for help in fabrication of samples. This work was founded by the Spanish Ministerio de Economía y Competitividad with project TEC2014-51902-C2-2-R. M.B. acknowledges funding by the Spanish Ministerio de Economía y Competitividad with contract RYC-2011- 08221. N.M.E. and A.A. have been supported by the NSF CAREER Award No. ECCS-0953311 and the AFOSR Grant No. FA9550-13-1-0204.

Received: ((will be filled in by the editorial staff))
Revised: ((will be filled in by the editorial staff))
Published online: ((will be filled in by the editorial staff))

[1] D. Schurig, J. J. Mock, B. J. Justice, S. A. Cummer, J. B. Pendry, A. F. Starr, D. R. Smith, *Science* **2006**, *314*, 977.

[2] J. Valentine, J. Li, T. Zentgraf, G. Bartal, X. Zhang, *Nat. Mater.* **2009**, *8*, 568.

[3] L. H. Gabrielli, J. Cardenas, C. B. Poitras, M. Lipson, *Nat. Photonics* **2009**, *3*, 12.

[4] U. Leonhardt, *Science* **2006**, *312*, 1777.

[5] J. B. Pendry, D. Schurig, D. R. Smith, *Science* **2006**, *312*, 1780.

[6] A. Alù, N. Engheta, *Phys. Rev. E* **2005**, *72*, 16623.

[7] D. Rainwater, A. Kerkhoff, K. Melin, J. C. Soric, G. Moreno, A. Alù, *New J. Phys.* **2012**, *14*, 13054.

[8] A. Alù, *Phys. Rev. B - Condens. Matter Mater. Phys.* **2009**, *80*, 1.

[9] P.-Y. Chen, A. Alù, *Phys. Rev. B - Condens. Matter Mater. Phys.* **2011**, *84*, 1.

[10] F. Monticone, A. Alù, *Phys. Rev. X* **2013**, *3*, 41005.

[11] J. Li, J. B. Pendry, *Phys. Rev. Lett.* **2008**, *101*, 203901.

[12] R. Liu, C. Ji, J. J. Mock, J. Y. Chin, T. J. Cui, D. R. Smith, *Science* **2009**, *323*, 366.

[13] H. F. Ma, W. X. Jiang, X. M. Yang, X. Y. Zhou, T. J. Cui, *Opt. Express* **2009**, *17*, 19947.

[14] N. Yu, P. Genevet, M. A. Kats, F. Aieta, J.-P. J.-P. Tetienne, F. Capasso, Z. Gaburro, *Science* **2011**, *334*, 333.

[15] A. V. Kildishev, A. Boltasseva, V. M. Shalaev, *Science* **2013**, *339*, 1289.

[16] N. Yu, F. Capasso, *Nat. Mater.* **2014**, *13*, 139.

[17] J. Zhang, Z. Lei Mei, W. Ru Zhang, F. Yang, T. Jun Cui, *Appl. Phys. Lett.* **2013**, *103*, 151115.

[18] N. Mohammadi Estakhri, A. Alù, *IEEE Antennas Wirel. Propag. Lett.* **2014**, *13*, 1775.

[19] B. Orazbayev, N. Mohammadi Estakhri, M. Beruete, A. Alù, *Phys. Rev. B* **2015**, *91*, 195444.

[20] N. Mohammadi Estakhri, C. Argyropoulos, A. Alù, N. M. Estakhri, C. Argyropoulos, A. Alu, *Philos. Trans. R. Soc. London* **2015**, 1.

[21] X. Ni, Z. J. Wong, M. Mrejen, Y. Wang, X. Zhang, *Science* **2015**, *349*, 1310.

[22] Y. Yang, L. Jing, B. Zheng, R. Hao, W. Yin, E. Li, C. M. Soukoulis, H. Chen, *Adv. Mater.* **2016**, DOI 10.1002/adma.201600625.

[23] P. H. Siegel, *IEEE Trans. Microw. Theory Tech.* **2002**, *50*, 910.

[24] M. Tonouchi, *Nat. Photonics* **2007**, *1*, 97.

[25] C. A. Balanis, *Antenna Theory: Analysis and Design*, Wiley, **2015**.

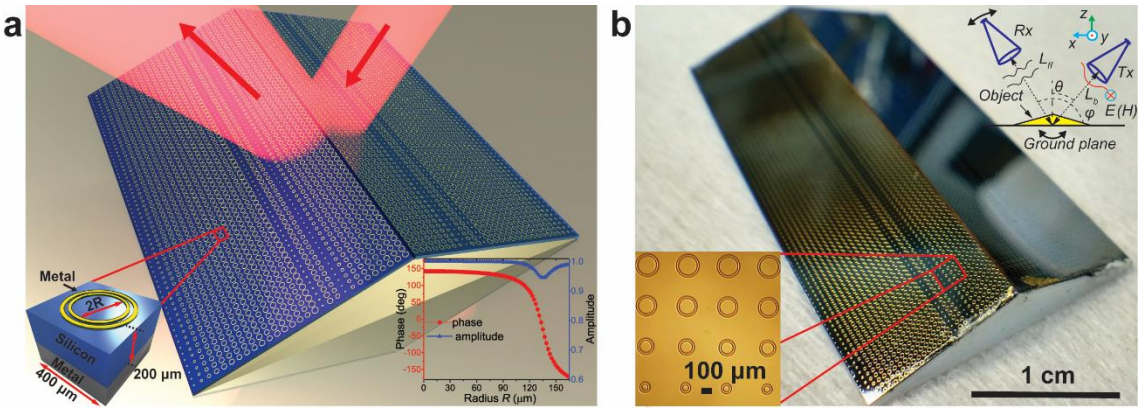


**Figure 1.** Schematic illustration and photographs of the fabricated metasurface cloak. a) 3D view of the cloak metasurface composed of an array of double coaxial metallic ring. Left inset: detail of a metasurface element with representative parameters. Right inset: amplitude and phase response of the unit cell as a function of the ring radius. b) Photograph of the fabricated cloak. Left inset: microscope picture showing a detail of the fabricated rings. Right inset: scheme of experimental set-up.

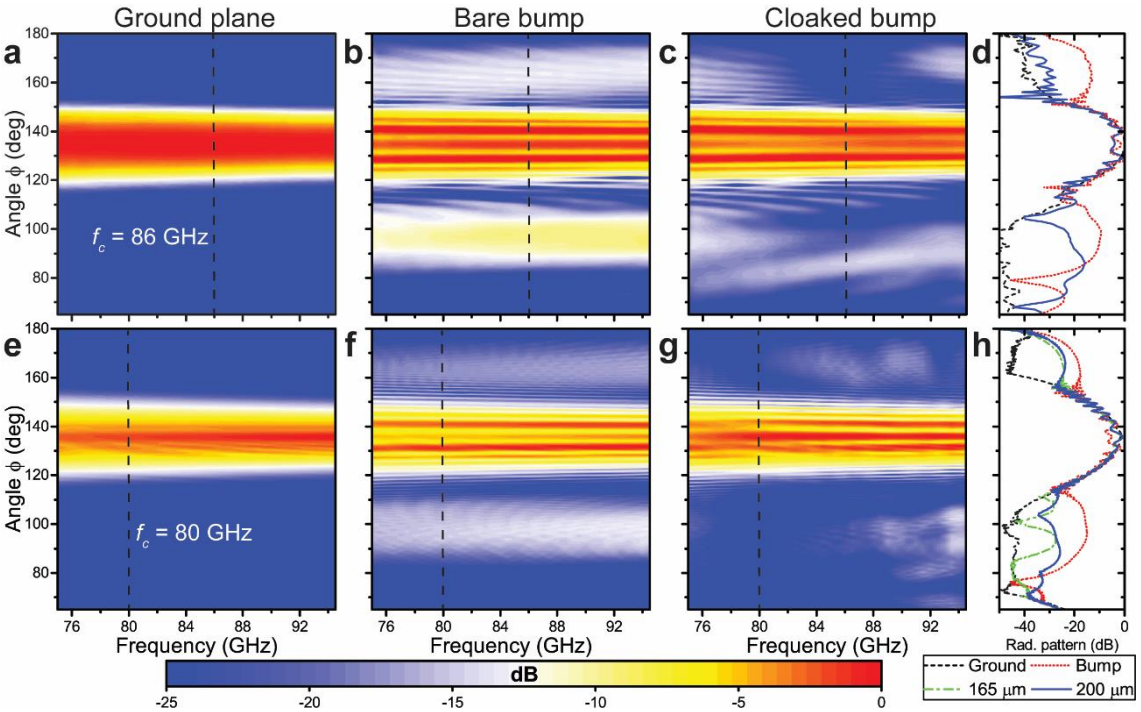


**Figure 2.** Radiation pattern for ground plane, bare bump and cloaked bump at the optimum incidence angle θ = 45° and *TE*-polarization. a-c) Experimental results. d) Experimental radiation patterns for all three cases at $f_c$ = 86 GHz. e-g) Simulation results. h) Numerical radiation patterns at frequency $f_c$ = 80 GHz.

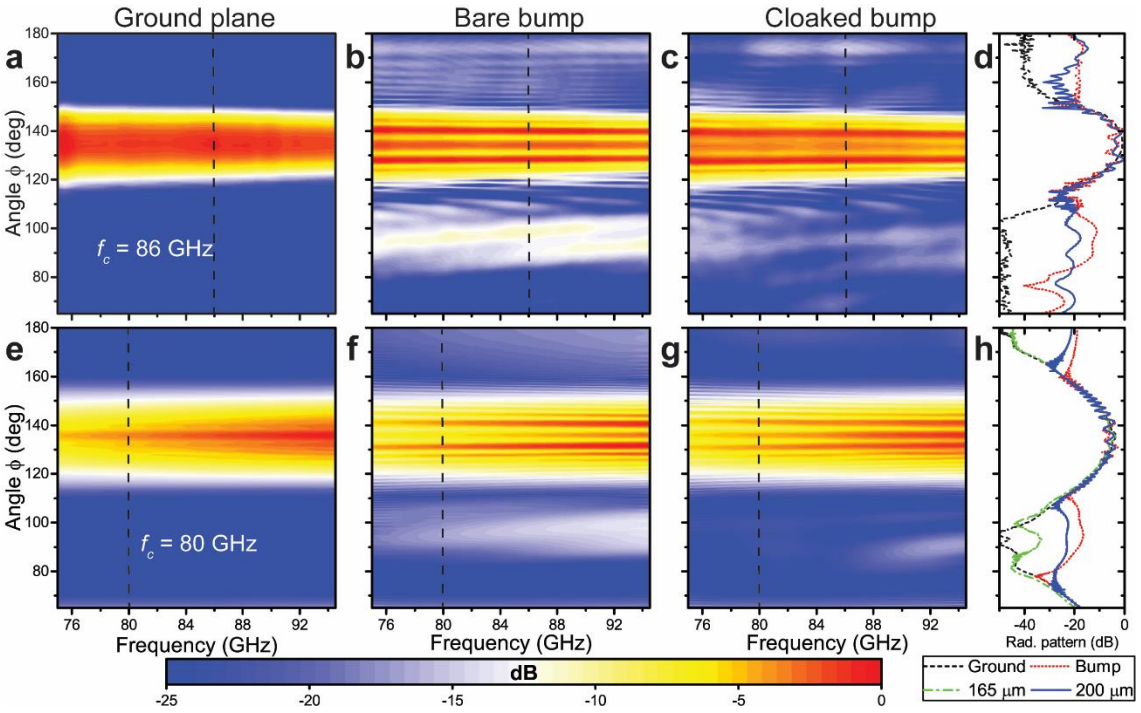

**Figure 3.** Radiation pattern for ground plane, bare bump and a cloaked bump at the optimum incidence angle θ = 45° and *TM*-polarization. a-c) Experimental results. d) Experimental radiation patterns for all three cases at $f_c$ = 86 GHz. e-g) Simulation results. h) Numerical radiation patterns at frequency $f_c$ = 80 GHz.

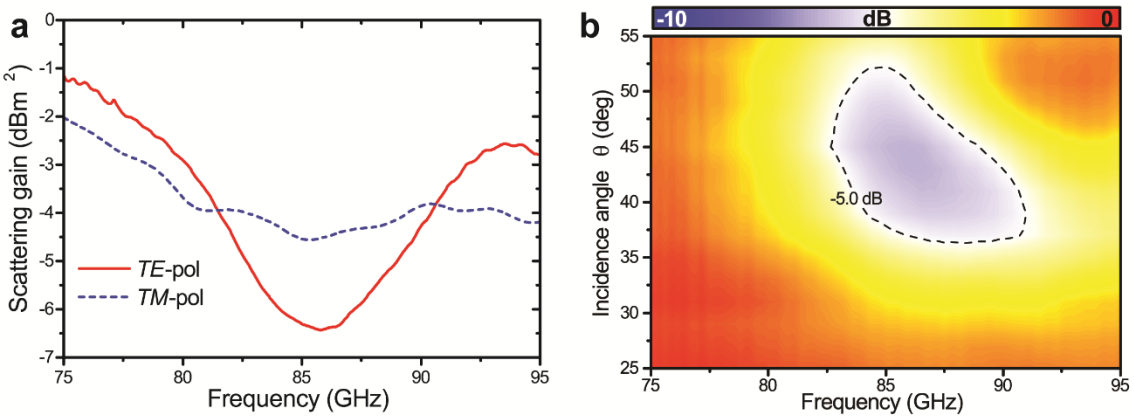


**Figure 4.** Experimental scattering gain. a**)** Experimentally measured scattering gain at the optimum incidence angle θ = 45° for the *TE*-polarization (solid red line) and for the *TM*-polarization (dashed blue line). b) Experimental scattering gain vs incident angle and frequency for *TE*-polarization.

**A metasurface carpet cloak for millimetre-wave range with polarization independent performance** is experimentally demonstrated. It is shown that the cloak is able to mimic the ground plane by fully restoring the amplitude and phase distributions for both *TE* and *TM* polarizations, with a relatively wide frequency and angular widths response.

**Keyword** Metamaterials

Bakhtiyar Orazbayev, Nasim Mohammadi Estakhri, Andrea Alù*, Miguel Beruete*

## Metasurface-based ultrathin carpet cloak for millimetre waves

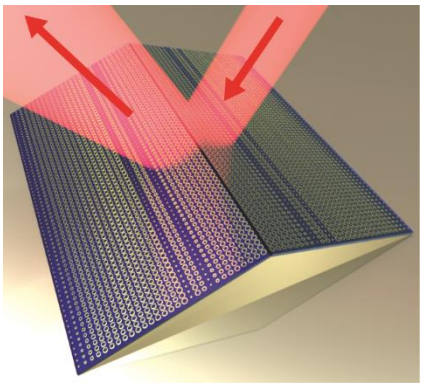

Copyright WILEY-VCH Verlag GmbH & Co. KGaA, 69469 Weinheim, Germany, 2013.

Supporting Information

# Metasurface-based ultrathin carpet cloak for millimetre waves

*Bakhtiyar Orazbayev, Nasim Mohammadi Estakhri, Andrea Alù*[*]*, Miguel Beruete*[*]

**Fabrication of cloaking metasurface.** The fabrication of the metasurfaces was made with photolithography followed by a lift-off procedure. The lift-off technique is a three-step process in which a photoresist film is first deposited and patterned, a metal layer is then grown and finally the resist sacrificial layer is stripped off in order to remove the undesired metal. In the first step, a double-side-polished (DSP), float-zone grown (FZ), high resistivity ($\rho > 10000$ Ω·m) silicon wafer with diameter 50.8 mm and thickness of 200 μm was cleaned and dehydrated. A thick layer of negative resist was then spin-coated, soft baked and exposed with a Suss MJB4 mask aligner. The UV exposure dose was carefully chosen to adjust the angle of the vertical walls of the resist. A positive angle would cause a later deposition of metal in the side-walls of the resist resulting in metal fence formation after the resist striping, whereas a too negative angle would compromise the accuracy of the process. With this technique a resolution of 1 μm can be reached, ensuring a minimal gap between two coaxial rings of 10 μm. After developing the resist, a 500 nm thick layer of copper and a 300 nm gold layer were sputtered. Although at the working frequency (0.08 THz) the skin depth does not exceed 300 nm the metal the thickness was fixed to 1 μm to ensure low losses, as was also done in the numerical calculations. The sputtering technique uses ionized argon plasma to attack the target material and strike out metal atoms that are deposited onto the sample. Since for this process the chamber pressure is relatively high (around 1.3 Pa), the deposition pattern is not completely directive, which can cause step coverage unless a sufficient negative angle is achieved during the

photolithography process. The sacrificial resist layer was removed with a striper based on a solution of tetra-methyl ammonium hydroxide (TMAH).

**Simulation set-up.** Full-wave simulations of the structure were performed using the transient solver of CST Microwave Studio™. The ground plane was emulated by using an electric boundary (perfect electric conductor) in the *xy* plane ($z = 0$). Given the symmetry of the structure, an electric (magnetic) symmetry for the *TE* (*TM*) polarization was applied in the *xz* plane in order to reduce computational time. A fine hexahedral mesh was applied with minimum cell length of 0.1 mm ($0.026\lambda_0$) and maximum of 0.35 mm ($0.09\lambda_0$). A thin silicon layer was used for the substrate with thickness $h = 200$ μm ($\approx\lambda_0/19$), dielectric permittivity $\varepsilon_r = 11.2$ and loss tangent $\tan\delta = 4.7\times10^{-6}$. Metallic rings were modelled as aluminium with conductivity $\sigma_{Al} = 3.56\times10^7$ S/m.

The structure was illuminated by an obliquely incident Gaussian beam with both *TE* and *TM* polarizations. To this end, an array of electric dipoles perpendicular (in-plane) to the incident plane was used with Gaussian distribution of amplitudes and phases, emulating a quasi-Gaussian beam distribution of the corrugated horn antenna with *TE* (*TM*) polarization. The array was placed at 500 mm ($133\lambda_0$) from the sample, the same distance as in the experiment. The radiation patterns were directly calculated by the built-in far-field monitors of CST Microwave Studio™.

To obtain the radar cross section and scattering gain the structure was illuminated by a plane wave source and periodic boundaries were used in *y*-axis direction with period $d = 400$ μm. The total RCS was calculated by integrating the RCS in the azimuthal *xz* plane, obtained by the built-in far-field monitors of CST Microwave Studio™.

**Experimental setups.** The scheme of the two experimental setups used in our work is shown in Supplementary **Figure S**3. In both setups corrugated high gain horn antennas were used as

transmitter (*Tx*) and receiver (*Rx*) and placed at the distances $L_b$ and $L_{ff}$ respectively. In first setup we used the AB millimetre vector network analyser (ABmm VNA) to measure the scattered *E*-field by capturing the scattering parameter $S_{21}$ in the range 75 - 95 GHz. The transmitter and the ground plane (a copper plate with dimensions 300×400 mm) with attached bump were both mounted on a rotational platform, and the whole structure was rotated in the range $\varphi = 45° - 180°$ (maximum available range due to the setup configuration) keeping the incidence angle constant. The transmitting antenna was placed at $L_b$ = 460 mm to ensure both uniform illumination of the structure and a beam waist diameter (67 mm) smaller than the ground plane (300 mm × 400 mm) to avoid diffraction. The receiver was placed at $L_{ff}$ = 3230 mm ($860\lambda_0$). With these distances we ensured that the measurements were done in the far-field region of the horn antennas (≈ 230 mm). The floor and walls were partially covered with absorbers in order to mimic anechoic chamber conditions. Furthermore, the setup was calibrated by recording the maximum reflected field from the ground plane when no object was presented. To this end, both transmitter and receiver were placed at the same angle 45°. This reflected field was subsequently subtracted from the measured reflected fields for other scattering angles.

Due to the ABmm VNA's characteristics the measurements were time consuming and were not suitable for bandwidth and angular span measurements. Therefore, another set-up based on an Agilent E3861C VNA was used to capture the scattering parameter $S_{21}$ in the range 75-95 GHz and in the range $\varphi = 60° - 180°$. In this set-up, transmitter and receiver were placed at the distances $L_b$ = 500 mm and $L_{ff}$ = 630 mm respectively. In this configuration the beam waist diameter (71 mm) is also smaller than the ground plane. Analogously to the first setup, a calibration was performed. Moreover, a software-based time-gating was applied to eliminate spurious reflections.

**Radar cross section extraction and scattering gain.** After the measurements were calibrated by subtracting the background contribution, the post-processed *S*-parameter values were converted to RCS (σ) values using the radar range equation:

$$|S_{21}|^2 = \frac{G_r G_t \lambda_0^2 \sigma}{(4\pi)^3 L_b^2 L_{ff}^2}$$

where *Gr* and *Gt* are gains of the receiver and transmitter respectively, and $L_b$ and $L_{ff}$ are the distances from the cloaked object to the receive and transmit antennas. The total RCS was found by integrating the RCS over measured angles (φ = 45°-180°).

The scattering gain ($dBm^2$) was calculated as the ratio between the RCS of the cloaked and bare bump:

$$G = 10\log\left(\frac{\sigma_{cloak}}{\sigma_{bump}}\right),$$

where $\sigma_{cloak}$ and $\sigma_{bump}$ are total scattering cross section for the cloaked and bare bump respectively.

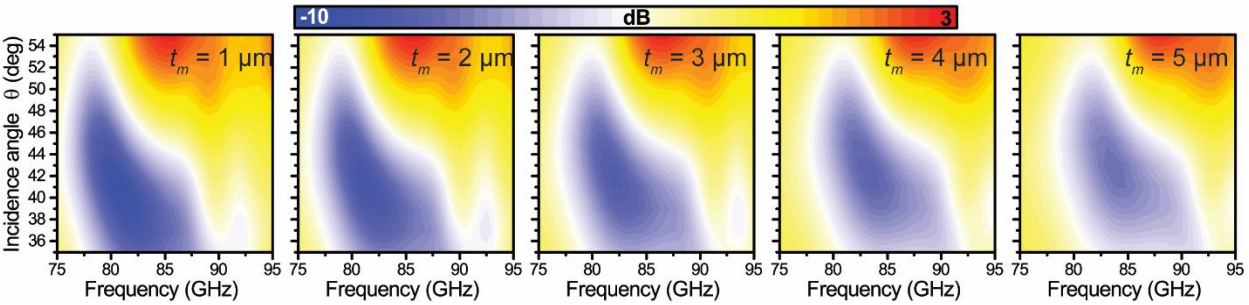


**Figure S1.** Numerical scattering gain vs incidence angle and frequency for different thicknesses of the metal rings.

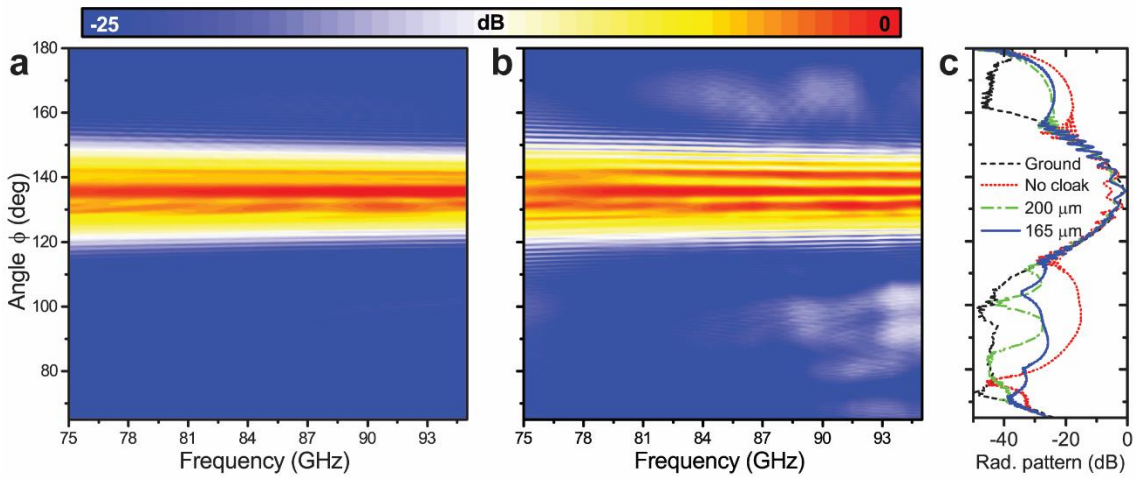


**Figure S2.** Radiation pattern for a cloaked bump at the optimum incidence angle θ = 45°. a**)** Numerical radiation pattern for a cloak with substrate thickness 165 μm. b) Numerical radiation pattern for a cloak with substrate thickness 200 μm. c) Numerical radiation patterns for substrate thickness 165 μm (green dash dotted curve) and 200 μm (blue solid curve) at frequency $f_c$ = 80 GHz.

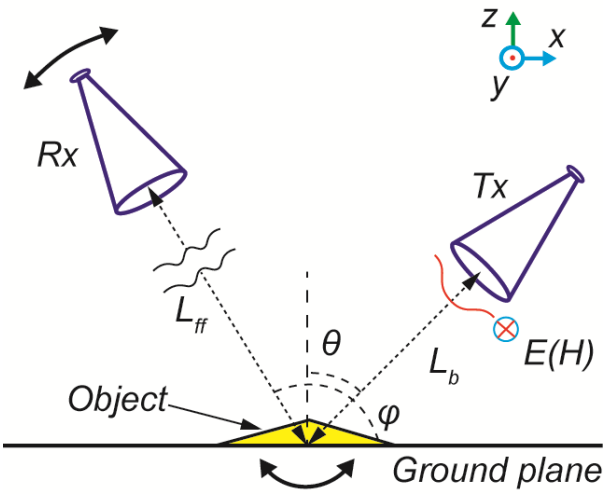


**Figure S3.** Schematic view of the experimental set-ups.